11th World Congress on Computational Mechanics (WCCM XI)
5th European Conference on Computational Mechanics (ECCM V)
6th European Conference on Computational Fluid Dynamics (ECFD VI)
E. Oñate, J. Oliver and A. Huerta (Eds)

NUMERICAL SIMULATION OF TRANSPIRATION COOLING WITH A MIXTURE OF THERMALLY PERFECT GASES

WOLFGANG DAHMEN, VALENTINA GERBER, THOMAS GOTZEN, SIEGFRIEG MÜLLER, MICHAEL ROM AND CHRISTIAN WINDISCH

Institut für Geometrie und Praktische Mathematik
RWTH Aachen University, Templergraben 55, 52056 Aachen, Germany

Key words: Transpiration Cooling, Porous Media, Darcy-Forchheimer, Compressible RANS, Finite Element-Finite Volume Coupling

Abstract. Transpiration cooling using ceramic matrix composite (CMC) materials is an innovative concept for cooling rocket thrust chambers. Numerical simulations of a carbon/carbon material mounted in the side wall of a hot gas channel have been performed. The coolant, air or argon, is driven through the porous material by a pressure difference between the coolant reservoir and the turbulent hot gas flow. A finite volume solver for the compressible Reynolds-averaged Navier-Stokes equations is coupled with a finite element porous medium solver. The results at Mach number $Ma = 0.3$ and hot gas temperature $T_{HG} = 420\,K$ are compared with experimental data.

1 INTRODUCTION

In future space transportation systems, the reduction of heat loads at the wall is an important design parameter. Since passive cooling techniques, such as radiation cooling, are limited and nonadjustable during flight, active solutions, e.g., transpiration cooling, might offer a promising alternative. In particular, such a technology would allow one to reduce the weight of the structural component. The basic idea of film, effusion and transpiration cooling is to inject a coolant through slits, boreholes or porous material into the hot gas flow boundary layer such that a coolant film develops. This leads to a significant reduction of the heat load at the wall.

Transpiration cooling, where the coolant is injected into the hot gas flow through a porous material, might offer advantages for the formation of stable films. The injection is driven by the pressure difference between the hot gas flow and the coolant reservoir. The hot gas in the boundary layer is displaced and a protective layer with lower temperature is formed on the surface of the cooled structure. As the complete boundary layer becomes thicker, the temperature and velocity gradients at the wall are getting smaller.

In addition, the low temperature of the gas close to the wall leads to a lower viscosity and thermal conductivity. Both effects lead to a significant reduction of the resulting wall heat flux and skin friction. The cooling efficiency might be intensified by using coolants with favorable properties, such as a low viscosity, a low thermal conductivity and a high specific heat capacity. Appropriate porous materials are currently under investigation [1]. Langener et al. [2] investigated transpiration cooling with CMC materials, in particular composite carbon/carbon (C/C) materials at sub- and supersonic speeds.

In the present work, we focus on the numerical simulation of cooling gas injected through a porous material into a hot gas channel flow. For this configuration, experimental data are available from Schweikert et al. [3] for the injection of air and argon, respectively. Argon as a nonflammable and nontoxic gas has been chosen to investigate the cooling effect of a gas which has a higher molecular weight than air. The simulations are carried out using separate solvers for the hot gas flow and the flow in the porous medium, respectively, that are directly coupled with each other through alternating data exchange at the interface. Since we are only interested in steady state solutions, the coupling is realized in a weak sense. This means, both solvers are applied alternately and converged to a steady state with respect to the coupling conditions generated from the solution of the other solver at this step of the iteration process. Concerning the hot gas flow, we use the adaptive parallel solver Quadflow [4], which solves the compressible Reynolds-averaged Navier-Stokes equations using the Menter SST turbulence model [5].

The porous medium flow is modeled by the continuity equation, the Darcy-Forchheimer equation and two temperature equations for both fluid and solid material. This model is discretized by a finite element scheme using the deal.II library [6]. In the following, we will refer to the two solvers as the flow solver and the porous medium solver, respectively.

The present paper is structured as follows: first of all, the governing equations for modeling both the hot gas flow and the porous medium flow are presented in Sect. 2. After describing the experimental and the numerical setup in Sect. 3.1 and 3.2, respectively, numerical results for the coupled simulation of the injection of air and argon through the porous material into the turbulent flow field are presented and compared with experimental data in Sect. 3.3. We conclude with a summary of the main results.

2 PHYSICAL MODELING

In this section, we briefly describe the equations required to simulate the hot gas flow and the models applied for the thermodynamic and transport properties. In addition, the modeling of the porous medium flow and the coupling of both flow solvers are described.

2.1 Hot gas flow

Governing equations. We shall consider non-stationary flows since this conveniently accommodates classical turbulence models. According to the physical problem investigated here, we are not interested though in time accurate computations but will rather consider time as a relaxation parameter. Specifically, turbulent flows can be described

by the Reynolds-averaged Navier-Stokes equations (RANS). In case of compressible flows with fluctuations in the density, these can be simplified by an additional Favre-averaging. We use an extended set of the Navier-Stokes equations which accounts for non-reacting mixtures of thermally perfect gases. Turbulent quantities of the Navier-Stokes equations resulting from the averaging process are modeled via the two-equations Menter SST model. With $\bar{\cdot}$ denoting Reynolds-averaged and $\tilde{\cdot}$ Favre-averaged quantities, the resulting dimensional equations using the Einstein summation convention read:

$$\frac{\partial \overline{\rho}}{\partial t} + \frac{\partial (\overline{\rho}\widetilde{v}_j)}{\partial x_j} = 0 \tag{1}$$

$$\frac{\partial \overline{\rho}_\alpha}{\partial t} + \frac{\partial (\overline{\rho}_\alpha \widetilde{v}_j)}{\partial x_j} = \frac{\partial}{\partial x_j} \overline{q}^D_{\alpha j} \tag{2}$$

$$\frac{\partial (\overline{\rho}\widetilde{v}_i)}{\partial t} + \frac{\partial (\overline{\rho}\widetilde{v}_i\widetilde{v}_j)}{\partial x_j} = -\frac{\partial \overline{p}}{\partial x_i} + \frac{\partial \overline{\tau}_{ij}}{\partial x_j} - \frac{\partial}{\partial x_j}\left(\overline{\rho}\tilde{R}_{ij}\right) \tag{3}$$

$$\frac{\partial (\overline{\rho}\widetilde{E})}{\partial t} + \frac{\partial \widetilde{v}_j(\overline{\rho}\widetilde{E} + \overline{p})}{\partial x_j} = \frac{\partial}{\partial x_j}\left(\overline{\tau}_{ij}\tilde{v}_i\right) - \frac{\partial}{\partial x_j}\left(\overline{q}_j + q^t_j + \overline{h}_\alpha \overline{q}^D_{\alpha j}\right) - \frac{\partial}{\partial x_j}\left(\overline{\rho}\tilde{R}_{ij}\tilde{u}_i\right) + \overline{\rho} D_j \tag{4}$$

$$\frac{\partial}{\partial t}\left(\overline{\rho}k\right) + \frac{\partial}{\partial x_j}\left(\overline{\rho}k\tilde{v}_j\right) = P_k - \beta_k \overline{\rho}\omega k + \frac{\partial}{\partial x_j}\left[\left(\mu + \sigma^\star_k \mu_t\right)\frac{\partial k}{\partial x_j}\right] \tag{5}$$

$$\frac{\partial}{\partial t}\left(\overline{\rho}\omega\right) + \frac{\partial}{\partial x_j}\left(\overline{\rho}\omega\tilde{v}_j\right) = P_\omega - \beta^\star \overline{\rho}\omega^2 + \frac{\partial}{\partial x_j}\left[\left(\mu + \sigma^\star_\omega \mu_t\right)\frac{\partial \omega}{\partial x_j}\right] + 2\left(1 - F_1\right)\frac{\sigma^0_\omega \overline{\rho}}{\omega}\frac{\partial k}{\partial x_j}\frac{\partial \omega}{\partial x_j} \tag{6}$$

No chemical source terms are included here as the temperatures in the flow field are expected to be low. With N_S denoting the number of species, the system is solved for $N_S - 1$ partial densities $\overline{\rho}_\alpha$, as the density of the remaining species may be computed from the global density $\overline{\rho} = \sum_{\alpha=1}^{N_S} \overline{\rho}_\alpha$. For closure of the system, the pressure $\overline{p}$ is calculated with the equation of state $\overline{p} = \sum_{\alpha=1}^{N_S} \overline{\rho}_\alpha R_\alpha \tilde{T}$, where the gas is considered to be a mixture of thermally perfect but calorically imperfect gases.

The Reynolds stress tensor $\overline{\rho}\tilde{R}_{ij}$ is modeled via the Boussinesq hypothesis [7]. The turbulent heat flux q^t_j is assumed to be proportional to the temperature gradient in analogy to Fourier's law, leading to $q^t_j \approx -c_P \frac{\mu_t}{Pr_t}\frac{\partial \tilde{T}}{\partial x_j}$. The turbulent Prandtl number Pr_t is set to the constant value $Pr_t = 0.9$. The turbulent viscosity μ_t and the transport term $\overline{\rho}D_j$ are modeled by the Menter SST turbulence model. Therefore, (5) and (6) are solved for the turbulence kinetic energy k and the turbulent dissipation ω. Details on the turbulence model and all related coefficients may be found in the literature, see [5, 7].

Thermodynamic and transport properties. All required quantities of the gas mixture are computed by considering the corresponding property of each species α and its particular contribution to the gas mixture, e.g., weighted by the mass fraction $X_\alpha = \overline{\rho}_\alpha / \overline{\rho}$. In this study, a gas mixture of five species air (N, N_2, O, O_2, NO) and argon is considered.

The formation enthalpies e^0_α and the corresponding internal energies $e_\alpha(\tilde{T})$ required to determine the total energy $\tilde{E} = \frac{1}{2}\tilde{v}_i\tilde{v}_i + \sum_{\alpha=1}^{N_S} X_\alpha e^0_\alpha + \sum_{\alpha=1}^{N_S} X_\alpha e_\alpha(\tilde{T}) + k$ are computed

from tabulated data [8], which are stored as piecewise polynomials so that a value for the internal energy may be obtained at any relevant and physically meaningful temperature.

The laminar shear stresses $\overline{\tau}_{ij}$ are determined by the usual Newtonian fluid assumption. This requires knowledge of the effective dynamic viscosity which is computed from the laminar and turbulent contributions. The laminar dynamic viscosity μ_l of the gas mixture is calculated with Wilke's semi-empirical mixing rule. Therefore, the dynamic viscosity of each species $\mu_{l,\alpha} = \mu_{l,\alpha}(T)$ is required, which is computed based on the Chapman-Enskog theory for pure monoatomic gases [9]. Due to large uncertainties in the determination of the Lennard-Jones parameters, the data differ depending on which data set is used. To ensure consistency of the data, as much data as possible are used from one of the available data sets [9–11]. The dynamic viscosities of the species are fitted as piecewise polynomials to simplify data handling.

Preceding investigations confirmed that the influence of the diffusion model on the wall heat flux is negligible so that a simple combined diffusion coefficient is used within this study. The diffusion flux of each species is approximated by Fick's law $\overline{q}^D_{\alpha j} = -\overline{\rho} D \frac{\partial}{\partial x_j}(\frac{\overline{\rho}_\alpha}{\overline{\rho}})$.

This assumption neglects pressure and thermal diffusion and considers only concentration gradients as the driving force. The local single diffusion coefficient D is calculated from the Lewis number, which is here defined as $Le = D\rho\frac{c_p}{\kappa}$. For the current purpose, the constant Lewis number for the argon-air combination may simply be approximated from the ratio of the binary diffusion coefficients $Le_{ac} = \frac{D_{ac}}{D_{aa}} Le_{aa}$.

The Lewis number for air is used as a reference value. The binary diffusion coefficients for air-coolant (ac) mixtures and for air-air (aa) mixtures are determined based on the Chapman-Enskog theory. In [9], approximated Lennard-Jones potential parameters for air mixtures and single species are published.

The laminar energy transport is driven by two forces, the thermal conduction $\overline{q}_j = \kappa\frac{\partial\tilde{T}}{\partial x_j}$ caused by temperature gradients and the transport of enthalpy $\overline{h}_\alpha = e(\tilde{T}) + \frac{\overline{p}}{\overline{\rho}}$ driven by diffusion. The thermal conductivity $\kappa_\alpha = \kappa_\alpha(\mu_\alpha, c_{V,\alpha})$ is calculated by means of the Euken correction for polyatomic molecules [11]. Wilke's semi-empirical mixing rule is applied to determine the mixture conductivity.

Boundary conditions. A sketch of the computational domain can be seen in Fig. 1. At the inflow boundary Γ_I, a turbulent profile for temperature and velocity is prescribed using the law of the wall. Air is modeled as a mixture of molecular nitrogen and oxygen ($X_{O_2} = 0.233$, $X_{N_2} = 0.767$). At the outflow boundary Γ_O, only the pressure is prescribed. The walls of the hot gas channel ($\Gamma_{W,HG}$) in

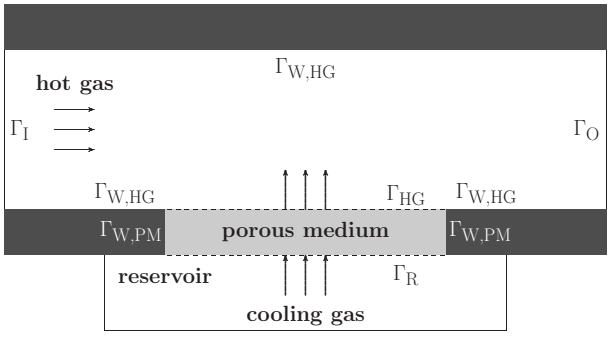

Figure 1: Computational domain of coupled fluid-porous medium problem.

the experiment are, in fact, neither adiabatic nor isothermal. For our computations, we asume the latter. Furthermore, no-slip boundary conditions are imposed. The boundary portion Γ_{HG} deserves special attention. Instead of no-slip conditions, we require

$$\mathbf{v}_{NS}|_{\Gamma_{HG}} = \mathbf{V}^* \,|_{HG}, \quad \rho_{NS} \,|_{\Gamma_{HG}} = \rho^* \,|_{\Gamma_{HG}}, \quad T_{NS} \,|_{\Gamma_{HG}} = T^* \,|_{\Gamma_{HG}}\,, \tag{7}$$

where $\mathbf{V}^*, \rho^*, T^*$ come from the porous medium flow and determine the total energy on Γ_{HG}.

2.2 Porous medium flow

Governing equations. In order to simulate the cooling gas injection into a hot gas flow through a porous material, a pressure-driven flow in a porous medium is modeled by taking the compressibility of the fluid, the velocity of the fluid and the thermal conduction in the fluid as well as in the solid into account. Only the coolant is considered in the porous medium flow, that means no hot gas enters the porous structure. The continuum model thus consists of the continuity equation, the Darcy-Forchheimer equation and two heat equations. We are particularly interested in properly capturing transport as well as non-equilibrium temperature effects.

In contrast to pure fluids, the porosity φ of the porous medium has to be accounted for in the continuum model. The porosity of a porous material is defined as the ratio of void space and the total volume of the medium. Here we assume that all the void space is connected. Averaging the fluid velocity over a volume V_f consisting only of fluid, the intrinsic average velocity $\mathbf{v}$ is obtained. This is related to the Darcy velocity $\mathbf{V}$, i.e., the average velocity with respect to a volume element V_m comprizing both solid and fluid material, by the porosity as $\mathbf{V} = \varphi\mathbf{v}$. The continuity equation for the fluid density ρ then reads

$$\varphi\frac{\partial\,\rho}{\partial\,t} + \nabla\cdot(\rho\mathbf{V}) = 0\,. \tag{8}$$

Quadratic drag is included in the momentum balance, resulting in the Darcy-Forchheimer equation

$$\rho\left(\frac{1}{\varphi}\frac{\partial\,\mathbf{V}}{\partial\,t} + \frac{1}{\varphi^2}(\mathbf{V}\cdot\nabla)\mathbf{V}\right) = -\nabla p - \mu\,\mathbf{K}_\mathbf{D}^{-1}\mathbf{V} - \rho\,\mathbf{K}_\mathbf{F}^{-1}|\mathbf{V}|\mathbf{V}\,. \tag{9}$$

Here, μ denotes the dynamic viscosity of the fluid, $\mathbf{K_D}$ the permeability tensor of the medium and $\mathbf{K_F}$ the Forchheimer coefficient, which is also a tensor. In the simulations presented in this paper, the contributions of the nonlinear Forchheimer term are small. The pressure p is determined by the equation of state for a thermally perfect gas $p = \rho T_f R$ with a frozen specific gas constant R and the fluid temperature T_f.

The temperatures T_s of the solid and T_f of the fluid are assumed to be in non-equilibrium. Therefore, two heat equations for both the solid and the fluid, respectively, are necessary. Since no convection takes place in the solid, we obtain

$$(1-\varphi)\rho_s c_s\frac{\partial\,T_s}{\partial\,t} = (1-\varphi)\nabla\cdot(\boldsymbol{\kappa_s}\,\nabla T_s) + h_v(T_f - T_s)\,, \tag{10}$$

where $\boldsymbol{\kappa_s}$ is the thermal conductivity tensor, ρ_s the constant density and c_s the specific heat capacity of the solid. Since the fluid is in contact with the solid, the exchange of heat is accounted for by the heat transfer coefficient h_v to be determined by experiments.

Since the fluid moves, convection occurs in the heat equation for the fluid

$$\varphi\rho c_{p,f}\left(\frac{\partial T_f}{\partial t}+\frac{1}{\varphi}\mathbf{V}\cdot\nabla T_f\right)=\varphi\nabla\cdot(\kappa_f\,\nabla T_f)+h_v(T_s-T_f)\,. \tag{11}$$

Here, κ_f is the thermal conductivity, which is equal in all directions and therefore a scalar, and $c_{p,f}$ is the specific heat capacity of the fluid at constant pressure.

Boundary conditions. For the boundary Γ of the domain occupied by the porous material, we have to distinguish between the *inflow boundary* Γ_R, where the cooling gas enters from the reservoir, and the *outflow boundary* Γ_{HG} of the porous medium, where the coolant leaves into the hot gas flow. In addition, we have to consider the solid walls $\Gamma_{W,PM}$ separating the porous medium from non-porous structure, see Fig. 1.

Pressure and temperatures at the inflow boundary are determined by the respective reservoir conditions. More precisely, denoting by T_b the temperature of the solid on the backside of the porous material, while p_c, T_c stand for reservoir pressure and temperature of the coolant, the boundary conditions on Γ_R read

$$p=p_c,\quad T_s=T_b,\quad T_f=T_c\qquad\text{on }\Gamma_R\,. \tag{12}$$

Concerning the outflow boundary Γ_{HG}, the influence of the hot gas flow is modeled by the boundary conditions

$$p=p_{HG}(t,\mathbf{x}),\quad -(\boldsymbol{\kappa_s}\nabla T_s)\cdot\mathbf{n}=h_{HG}(T_s-T_{HG}(t,\mathbf{x})),\quad V_y=\frac{\dot m}{\frac{p_{HG}}{T_{HG}R}A_{PM}}\quad\text{on }\Gamma_{HG} \tag{13}$$

with the hot gas pressure $p_{HG}(t,\mathbf{x})$ and temperature $T_{HG}(t,\mathbf{x})$, which may vary in time and space, the mass flux of the coolant $\dot m$ measured in the experiments and the surface area A_{PM} of the porous material. The heat transfer coefficient h_{HG} describes the heat exchange between the solid part of the porous material and the hot gas flow ($\neq h_v$!). It strongly depends on the injected coolant mass flux. Therefore, h_{HG} is modeled following the approach by Kays et al. [12].

The bordering walls $\Gamma_{W,PM}$ are assumed to be adiabatic, i.e., $\nabla T_s\cdot\mathbf{n}=0$ and $\nabla T_f\cdot\mathbf{n}=0$.

2.3 Coupling both flow regimes

We are ultimately interested in finding solutions in both flow regimes arising from the mutual interactions between both media. This interaction takes place at the boundary portion Γ_{HG} and results in a fully coupled system where the velocity field $\mathbf{V}$, fluid density ρ and structure temperature T_s from the porous medium enter as data for the hot

gas channel flow, while the temperature T_{HG} and pressure p_{HG} of the hot gas flow are transferred to the porous medium flow. This coupling strategy does not allow for any of the main flow gas to penetrate into the porous material. The stationary *equilibrium solution* of the coupled system at iteration step n is then determined by the continuity of the pressure at the interface, i.e., $\left| p^n_{NS} \,|_{\Gamma_{HG}} - p^n_{PM} \,|_{\Gamma_{HG}} \right| \leq \varepsilon$ for a given tolerance $\varepsilon > 0$.

Since we are only interested in steady state solutions, stationary solutions at the current iteration step are computed by alternating between both solvers. Therefore, the iteration process can be summarized as follows:
step 1: initialize flow solver → **step 2:** transfer data to porous medium solver → **step 3:** converge porous medium solver → **step 4:** transfer data to flow solver → **step 5:** converge flow solver → **step 6:** perform grid adaptation in the flow solver → **step 7:** stop if convergence criterium for pressure continuity is fulfilled or return to step 2

3 RESULTS

Two-dimensional simulations of coolant injection through porous material are carried out based on the above coupling strategy. The results are compared with results from hot gas channel experiments. Beforehand, we briefly describe the setup of the experiments conducted by Schweikert et al. [3] and discuss the numerical setup.

3.1 Experimental setup

Schweikert et al. [3] carried out experiments using carbon/carbon (C/C) ceramics as porous material. C/C material is a ceramic matrix composite (CMC) where both fibers and matrix are made from carbon. Temperatures are measured at locations in the material with different depths. For the experiments, the porous material is mounted into the sidewall of a subsonic wind tunnel. On the backside of the C/C material, a coolant reservoir is attached. The experimental setup is shown in Fig. 2. The test section is $1.32\,m$ long with the C/C material beginning $0.58\,m$ downstream from the entrance, the height is $90\,mm$ and the width $60\,mm$. The C/C probe measures $61\,mm \times 61\,mm$ and is

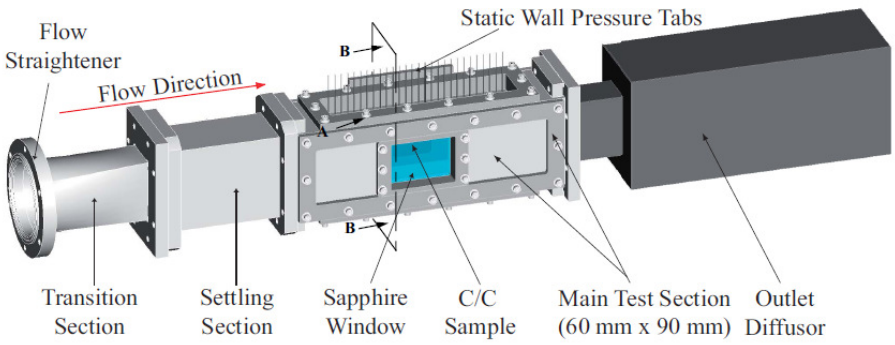

Figure 2: Experimental setup by Langener et al. [2].

Mach number	Ma	0.3
density	ρ_{HG}	$0.8\,\frac{kg}{m^3}$
total temperature	$T_{t,HG}$	$420\,K$
pressure	p_{HG}	$97\,kPa$
cool. mass flow rate	$\dot{m}$	$5.88\,\frac{g}{s}$
reservoir pressure	p_R	$615\,kPa$
cool. reservoir temp.	T_c	$296.3\,K$
backside temp.	T_b	$300.4\,K$

Table 1: Flow conditions.

throughflow dir.		parallel
porosity	φ	0.11
density	ρ_s	$1.14\,\frac{kg}{m^3}$
spec. heat capacity	$c_{p,s}$	$622\,\frac{J}{kgK}$
eff. therm. conduct.	k_s	$13.5\,\frac{W}{mK}$
permeability	K_D	$3.13 \cdot 10^{-13}\,m^2$
Forchheimer coeff.	K_F	$4.86 \cdot 10^{-8}\,\frac{1}{m}$

Table 2: Porous material parameters.

$15\,mm$ thick. The experiments are described in detail in Langener et al. [2].

The flow conditions in the hot gas channel and in the porous medium are summarized in Tab. 1, whereas Tab. 2 lists the parameters concerning the C/C material. The C/C material is produced by the DLR Stuttgart [1]. The probe used in the experiments corresponding to the simulations presented here is mounted into the wall in such a way that the flow through the material is parallel to one layer of the ceramic fibers.

3.2 Numerical setup

We apply the weak coupling of the finite volume solver Quadflow with the finite element porous medium solver on the boundary Γ_{HG} described in Sect. 2.3.

The finite element solver for the porous medium flow is implemented using the deal.II library. Details on this library can be found in Bangerth et al. [6]. The porous material is discretized by an equidistant coarse grid with 257×65 degrees of freedom. That is, because of the uniform porosity, no local grid adaptation is performed in the porous medium domain. The coarse grid for the flow solver comprises about 15,000 grid cells. The grid lines are concentrated towards the wall using a stretching function. The final adaptive grid after eight adaptations (and consequentially eight coupling iterations) consists of about 90,000 grid cells. Details on the discretization and the solution strategy in both flow regimes as well as a convergence study can be found in [13].

3.3 Numerical results

In this section, we first present the distribution of several quantities in the hot gas flow and in the porous material provided by the two-dimensional simulations. These computational results are then compared with experimental data from Schweikert et al. [3].

The temperature in the hot gas flow in the region of the porous material injection is shown in Fig. 3. A coolant film created by the injection through the porous material with increasing thickness over the length of the probe can be seen. Further downstream from the injection, the temperature in the coolant layer increases, mainly due to turbulent mixing. The film created by the injection of air is thicker compared with the argon injection, due to the higher molecular weight and therefore the higher density of the

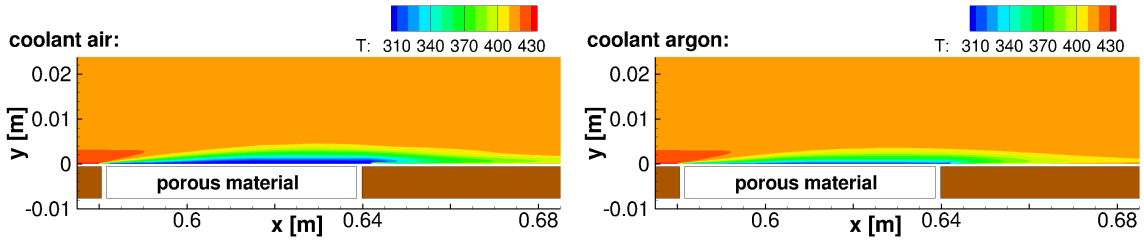

Figure 3: Temperature in the hot gas channel for injection of air (left) and argon (right).

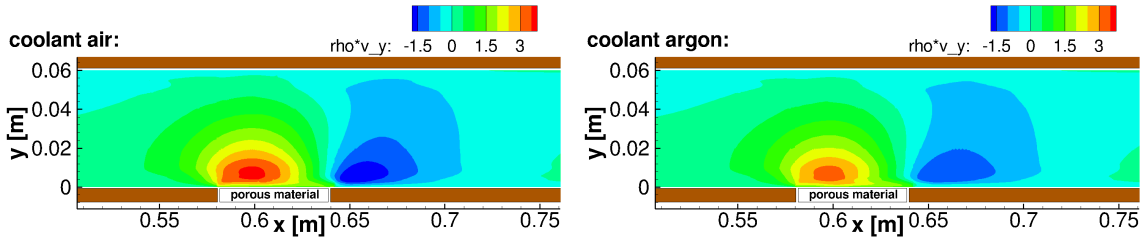

Figure 4: Wall-normal momentum in the hot gas channel for injection of air (left) and argon (right).

latter. Since the mass fluxes are the same, the volume flux of air which is injected is higher. This leads to a thicker coolant film and a better protection of the wall.

Fig. 4 shows the wall-normal momentum of the injection. A strong effect from the injection on more than half the channel height can be observed. Especially above the leading edge of the porous material, a high momentum appears. This results from the injection being an obstacle for the hot gas flow. The latter has to detach from the wall and flow around the injection, leading to a high wall-normal momentum. Considering the air injection, a higher wall-normal momentum can be seen because of the coolant film being thicker. Therefore, the hot gas flow is displaced further away from the wall.

In the following, we will discuss the flow field in the porous medium, beginning with the density distribution, see Fig. 5. Due to higher pressure in the coolant reservoir, the density evolves from higher values there to lower values on the hot gas side. There are no significant changes according to the run length x of the hot gas flow, the results are quasi one-dimensional. As mentioned before, the density of air is smaller compared with argon due to the lower molecular weight.

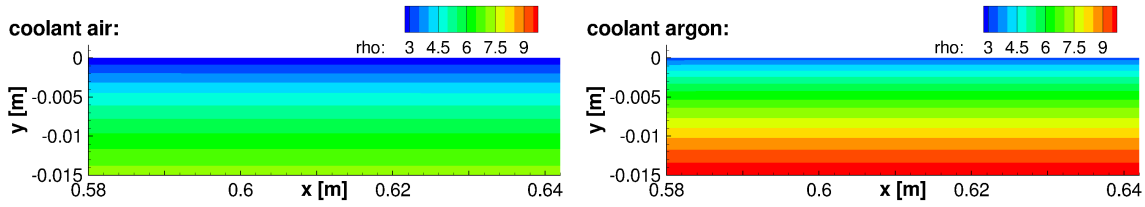

Figure 5: Density of fluid in porous material for injection of air (left) and argon (right).

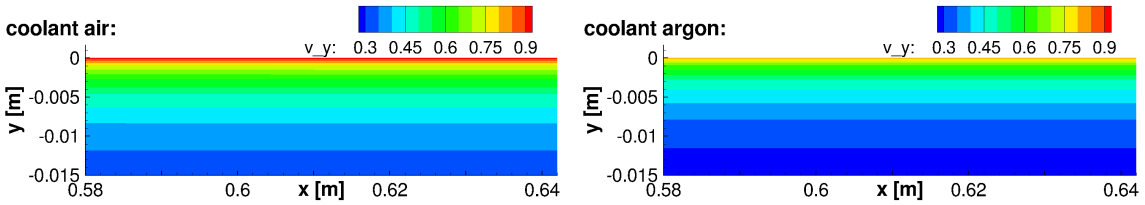

Figure 6: Darcy velocity in porous material for injection of air (left) and argon (right).

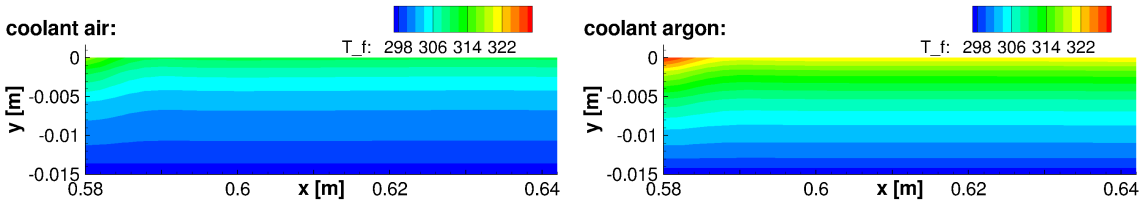

Figure 7: Temperature of fluid in porous material for injection of air (left) and argon (right).

The Darcy velocities resulting from the given pressure difference are shown in Fig. 6. According to the steeper pressure gradient close to the hot gas flow, the velocity increases. Again, there is no noticeable dependence in direction of the hot gas flow even though, due to the injection, there is a pressure drop in the hot gas flow. However, the overall pressure difference in the hot gas channel is small compared with the one in the porous medium that is necessary to drive the coolant through the C/C material. Comparing air and argon again, the lower density of air leads to higher Darcy velocities.

The temperature of the coolant inside the porous material is shown in Fig. 7. On its way through the porous wall, the coolant absorbs heat from the structure. On the hot gas side, the solid structure is hotter at the leading edge of the porous material and cooler further downstream because of the developing coolant film in the hot gas flow. This leads to the fluid becoming cooler there, too. We have seen before that, due to the lower molecular weight of air, the velocity and the volume flux are higher when air is injected. In addition, the specific heat capacity of air is about twice as large compared with argon. Therefore, the air does not heat up that much inside the porous material.

The temperature of the solid is gener-

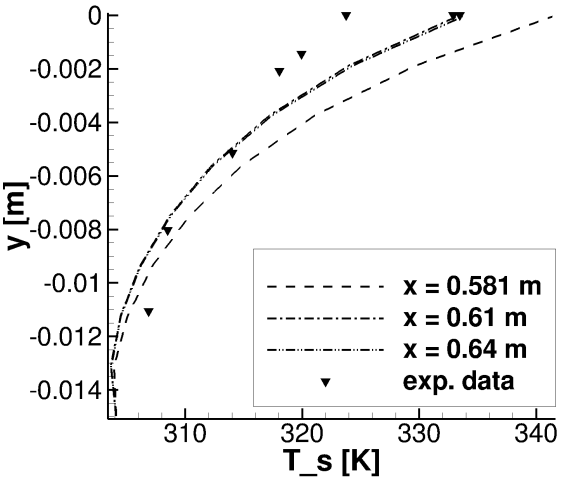

Figure 8: Solid temperature in the porous material at $x_1 = 0.581\,m$, $x_2 = 0.61\,m$ and $x_3 = 0.64\,m$ compared with experimental results for the injection of argon.

ally higher than the temperature of the fluid, but due to the strong coupling with the fluid temperature, the distribution shows essentially the same qualitative behavior.

In Fig. 8, the temperature of the solid taken at different y positions in the porous material is compared with experimental data in the case of argon injection. Schweikert et al. [3] placed thermocouples in different depths of the C/C material. The temperature at the hot gas side decreases in streamwise direction of the hot gas flow. Four thermocouples are placed at the surface of the porous material. All four are shown in the figure and therefore illustrate the variations in the measurements across the surface. The thermocouples at different depths in the C/C material cannot be placed above each other and are distributed over the whole cross-section.

4 CONCLUSION

The numerical investigations confirm that our finite element solver is suitable for simulating porous medium flow. Detailed insight into the distribution of temperature and flow in the porous material can be derived from the numerical results, where experimental results are limited due to the small extent of the porous material. The placement of measurement devices into such a small regime is very difficult and their distance from each other is limited. The comparison with experimental data confirms that the porous medium solver adequately reproduces the temperature distribution in the porous material. Nevertheless, there is a strong dependence on parameters like the heat exchange coefficients, which have yet to be determined by experiments.

We emphasize that common restrictive assumptions for modeling transpiration cooling are not used here. An example is one-dimensional modeling of the temperatures in the porous medium. The results presented here show a strong variation especially in streamwise direction. Additionally, often the temperatures of the fluid and the solid part of the porous medium are assumed to be in equilibrium. Even considering that the results presented here are vague in respect to the heat transfer between solid and fluid due to the lack of exact measurements of the heat transfer coefficients, it is fair to say that they show a significant difference between both temperatures.

Coupling of porous medium flow to pure fluid flow is a field of research which lacks in both theoretical investigations and practical application of numerical tools. To the authors' knowledge, there has been no approach of performing a fully coupled simulation of transpiration cooling so far. The weak coupling using boundary conditions performed in this study leads to convergence and reasonable results.

The simulation of two different coolants stressed the importance of a proper selection of the cooling gas. The low density of light coolants will lead to a thickened cooling film. This results in lower temperature gradients in the boundary layer and reduced heat fluxes.

Acknowledgment. Financial support has been provided by the German Research Foundation (Deutsche Forschungsgemeinschaft - DFG) in the framework of the Sonderforschungsbereich Transregio 40.

REFERENCES

[1] Selzer, M., Langener, T., Hald, H. and von Wolfersdorf, J. Production and Characterization of Porous C/C Material. In: N.A. Adams, R. Radespiel, T. Sattelmayer, W. Schröder, B. Weigand (Eds.), *Annual Report SFB-TRR40 2009*, München, pp. 75–85 (2009).

[2] Langener, T., von Wolfersdorf, J., Selzer, M. and Hald, H. Experimental investigations of transpiration cooling applied to C/C material. *Intl. J. Thermal Sc.* (2012) **54**:70–81.

[3] Schweikert, S., von Wolfersdorf, J., Selzer, M. and Hald, H. SFB-TRR40 project A5, private communication (2013).

[4] Bramkamp, F., Lamby, Ph. and Müller, S. An adaptive multiscale finite volume solver for unsteady and steady state flow computations. *J. Comp. Phys.* (2004) **197**(2):460–490.

[5] Menter, F.R. Two-Equation Eddy-Viscosity Turbulence Models for Engineering Applications. *AIAA J.* (1994) **32**(8):1598–1605.

[6] Bangerth, W., Hartmann, R. and Kanschat, G. deal.II - a general-purpose object-oriented finite element library, *ACM Trans. Math. Softw.* (2007) **33**(4):24/1–24/27.

[7] Noureldin, K. Turbulent Flow Simulations of a Mixture of Perfect Gases. *Master thesis, RWTH Aachen* (2012).

[8] Stull, D.R. and Prophet, H. JANAF thermochemical tables [electronic source]. National Institute of Standards and Technology (2011).

[9] Bird, R.B., Stewart, W.E. and Lightfoot, E.N. *Transport Phenomena*. John Wiley & Sons, Inc. (2007).

[10] Cloutman, L.D. A Database of Selected Transport Coefficients for Combustion Studies. Lawrence Livermore National Laboratory (1993).

[11] Hirschfelder, J.O., Curtiss, C.F. and Bird, R.B. Molecular Theory of Gases and Liquids. John Wiley & Sons, Inc. (1965).

[12] Kays, W., Crawford, M. and Weigand, B. *Convective Heat and Mass Transfer*. McGraw-Hill, New York, 4th edition (2005).

[13] Gotzen, T. Numerical investigation of film and transpiration cooling. Diss. RWTH Aachen (2013).